A General Approach to One-Pot Fabrication of Crumpled Graphene-Based Nanohybrids for Energy Applications

Shun Mao,[†,§] Zhenhai Wen,[†,§] Haejune Kim,[†] Ganhua Lu,[†] Patrick Hurley,[‡] and Junhong Chen[†,*]

[†]Department of Mechanical Engineering, University of Wisconsin—Milwaukee, 3200 North Cramer Street, Milwaukee, Wisconsin 53211, United States and [‡]Global Technology and Innovation, Power Solutions, Johnson Controls Inc., 5757 North Green Bay Avenue, Milwaukee, Wisconsin 53209, United States. [§]These authors contributed equally to this work.

ABSTRACT

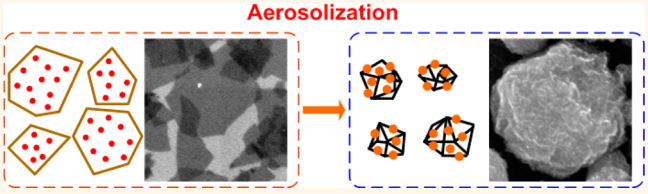

Crumpled graphene oxide (GO)/graphene is a new type of carbon nanostructure that has drawn growing attention due to its three-dimensional open structure and excellent stability in an aqueous solution. Here we report a general and one-step approach to produce crumpled graphene (CG)—nanocrystal hybrids, which are produced by direct aerosolization of a GO suspension mixed with precursor ions. Nanocrystals spontaneously grow from precursor ions and assemble on both external and internal surfaces of CG balls during the solvent evaporation and GO crumpling process. More importantly, CG—nanocrystal hybrids can be directly deposited onto various current-collecting substrates, enabling their tremendous potential for energy applications. As a proof of concept, we demonstrate the use of hybrid electrodes of CG—Mn_3O_4 and CG—SnO_2 in an electrochemical supercapacitor and a lithium-ion battery, respectively. The performance of the resulting capacitor/battery is attractive and outperforms conventional flat graphene-based hybrid devices. This study provides a new and facile route to fabricating high-performance hybrid CG—nanocrystal electrodes for various energy systems.

KEYWORDS: crumpled graphene · nanocrystal · nanohybrid · aerosolization · electrochemical supercapacitor · lithium-ion battery

Graphene oxide (GO) is a promising precursor for the creation of carbon-based nanostructures because it can be synthesized in large quantities by oxidizing inexpensive graphite powders and can be reduced through different methods to obtain tailored properties by controlling reduction conditions.[1−4] Due to the unique properties and potential applications of GO/graphene,[5−7] there is a great demand in the fabrication and assembly of designed architectures based on GO/graphene patterning, stacking, folding, and scrolling.[8−14] It was recently reported that aqueous GO sheets can be converted into crumpled graphene (CG) balls by capillary force associated with rapid solvent loss and physical deformation through an aerosolization process, from which GO is transformed from a two-dimensional (2D) sheet to a three-dimensional (3D) structure.[15,16] The as-produced CG is of great interest for fundamental scientific research and practical technological applications. First of all, the CG structure exhibits significantly enhanced specific surface area and possesses excellent stability under redispersion or other material processing treatments. Additionally, the synthetic method is facile and suitable for scalable continuous manufacturing. Finally, the controlled deformation of 2D graphene nanostructures can markedly increase reactive sites and can be further used for tuning the reaction barrier and reaction energetics of graphene, which opens up new opportunities for various applications as was demonstrated in *Nature* by R. Ruoff.[17]

The performance of a CG ball could be further enhanced through decoration or modification with various functional nanostructures. Such CG-based nanohybrids are envisaged to synergistically offer unique properties of both crumpled graphene and functional nanostructures, providing tremendous opportunities for improving and expanding applications.[18] For instance, it was reported that cargo-filled graphene nanosacks could be manufactured by aerosolizing GO suspension and nanoparticle mixtures.[19] However, research into CG is still in its infant stage, and methods for controlled functionalization of CG are yet to be developed. In fact, the lack of an efficient and general synthetic method represents a huge challenge to implement such CG-based hybrids for practical applications.

* Address correspondence to jhchen@uwm.edu.

Received for review June 25, 2012 and accepted July 28, 2012.

Published online July 29, 2012
10.1021/nn302818j

We herein report a general approach for one-step synthesis of nanohybrids of CG decorated with various nanocrystals of precious metals (*e.g.*, Pt, Ag) and metal oxides (*e.g.*, SnO_2, Mn_3O_4). The novelty in the present method is that nanocrystals are locally crystallized and grown *in situ* on the surface of CG sheets during the solvent evaporation and GO crumpling process, which is quite different from previously reported methods that mix presynthesized nanoparticles with GO suspension before the aerosolization process. In a typical synthesis, precursor ions (*e.g.*, Mn^{2+}, Sn^{4+}, Ag^+, and $[PtCl_6]^{2-}$) were dissolved in a GO suspension, which is then aerosolized and dried through a tube furnace by using an ultrasonic nebulizer. CG ball-based hybrids with different nanocrystals can be fabricated during this process. Of more practical significance, the product CG-based nanohybrids can be collected onto various types of substrates, enabling a direct route to fabricate binder-free electrodes for various energy storage and conversion devices, such as supercapacitors, lithium-ion batteries, and solar cells.

RESULTS AND DISCUSSION

CG−Nanocrystal Hybrids from Aerosolization of GO Suspension Mixed with Precursor Ions. Figure 1 shows the experimental setup for producing CG−nanocrystal hybrids using an aerosolization system. An aqueous dispersion of GO sheets with precursor ions was nebulized to generate aerosol droplets that flowed through a tube furnace preheated at 600−700 °C by an Ar/H_2 carrying gas. Because the average size of generated droplets was around 1.7 μm due to the high working frequency of the ultrasonic nebulizer (2.4 MHz), the solvents rapidly evaporated in the tube furnace, leading to the shrinkage of GO sheets and the subsequent compression of GO sheets into crumpled balls with a submicrometer size. Simultaneously, precursor ions adsorbed on the surface of GO sheets could be decomposed or reduced during the GO sheets' evaporation and crumpling process, leading to the loading of nanocrystals on the CG surface. Because of the high temperature, GO sheets were also partially reduced, as indicated by the color change from brown to black.

To investigate the morphology of the prepared CG−nanocrystal hybrids, SEM imaging was carried out and results are shown in Figure 2. Without the precursor, bare CG balls can be produced by this method, which is consistent with previous reports.[15,16] SEM images (Figure 2a,b) indicate that each of the CG balls is formed by a single piece of GO sheet, and in general, a larger GO sheet led to a CG ball with a larger diameter. The GO used in this study had a wide size distribution ranging from tens of nanometers to several micrometers, and the CG balls show a size distribution from 50 to 600 nm with a peak size at 200 nm (Figure 2c, red curve). On the basis of experimental results, the size of the CG balls was mainly dependent on the size of the initial GO sheets as well as the number of layers of the GO or GO thickness. This observation agrees well with previous reports (Supporting Information, Figure S1).[16]

To create a hybrid nanostructure of GO−nanocrystals, precursor ions were intentionally introduced as the source of nanocrystals, and the original idea of the design was to use the high temperature during the GO evaporation and crumpling to promote the nanocrystal growth on the surface of GO. Because precursor ions were adsorbed on the surface of the GO sheet, the GO sheet worked as a substrate for the localized crystallization or thermal decomposition. The product hybrid structures suggested that nanocrystals successfully grew on the surface of GO sheets during the GO evaporation and crumpling even though the GO flight time was as short as 1−2 s in the tube furnace.

SEM images (Figure 2e−l) reveal that various nanocrystals, including Mn_3O_4, SnO_2, Ag, and Pt nanocrystals, are uniformly deposited on the surface of CG balls, indicating the local growth of nanoparticles during the GO aerosolization and crumpling process. It should be noted that, at the macroscopic level, the CG−nanocrystal ball surface is smoother than that of the bare CG ball. This change in the surface smoothness of the CG ball can be attributed to the filling of nanocrystals in the innerspace of folded CG and the interspace between the folded CG sheet, as confirmed by TEM images (Figure 3). The CG−nanocrystal hybrids have a wide size distribution from 50 to 500 nm with a peak size at 150 nm (Figure 2c, blue curve). The nanocrystal size ranges are also plotted in Figure 2d. It was demonstrated that the nanocrystal size was variable depending on chemical properties of the ion source, the reaction temperature, and the precursor concentration. On the basis of measurements from SEM and TEM images, the sizes of nanocrystals on CG are 20 ± 10, 3 ± 1, 60 ± 30, and 18 ± 5 nm for Mn_3O_4, SnO_2, Ag, and Pt, respectively. It is proposed that different precursors can result in different reactions, as shown in reactions (1)−(3). For transition metal oxides, the metal ions initially adsorbed on the GO surface *via* electrostatic interactions, and the subsequent drying and annealing treatments resulted in the formation of transition metal oxides on CG. For precious metals, the metal ions can be reduced or decomposed *in situ* on the surface of CG.

$$GO + M^{a+} \rightarrow GO/M^{a+} \rightarrow G + M_xO_y \quad (M = \text{transition metal}) \qquad (1)$$

$$GO + Ag^+ + H_2 \rightarrow G + Ag \qquad (2)$$

$$GO + [PtCl_6]^{2-} \rightarrow G + Pt \qquad (3)$$

For chemical synthesis of inorganic nanocrystals, a surface surfactant is commonly used to control the size and morphology of the nanocrystal. Therefore, to investigate the surfactant function in this aerosolization

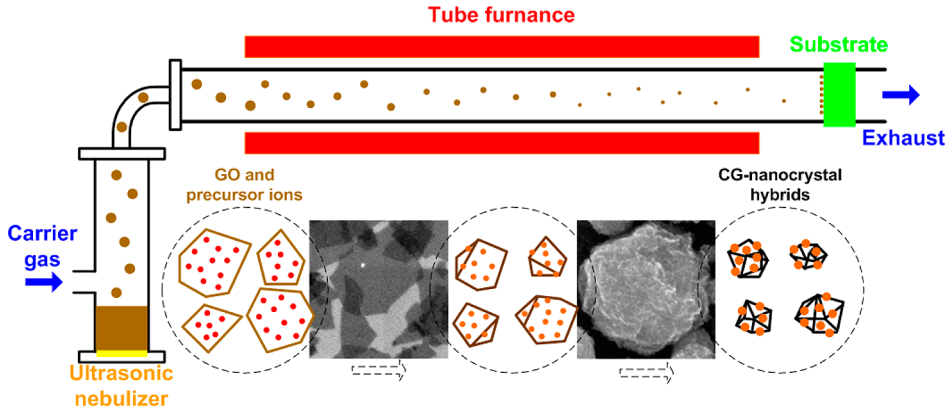

Figure 1. Preparation of CG−nanocrystal hybrids by rapid compression of GO sheets in evaporating aerosol droplets and simultaneous chemical reactions for growth of nanocrystals on the CG surface. Schematic illustration of the experimental setup and the aerosolization/high-temperature-induced GO crumpling and nanocrystal growth process.

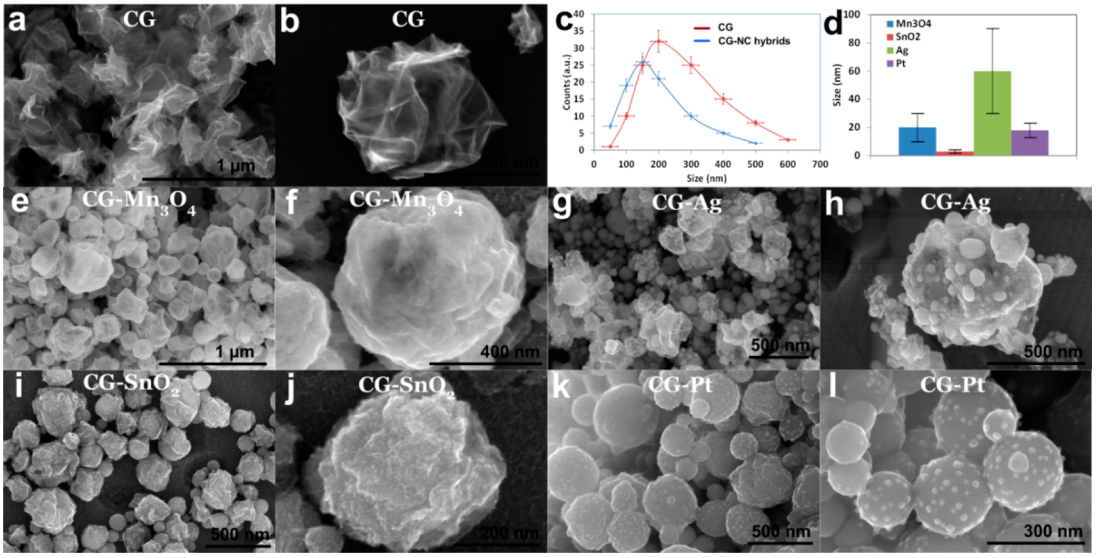

Figure 2. SEM images of bare CG and CG−nanocrystal hybrids: (a,b) bare CG balls; (e,f) CG−Mn_3O_4 nanocrystal hybrids; (g,h) CG−Ag nanocrystal hybrids; (i,j) CG−SnO_2 nanocrystal hybrids; (k,l) CG−Pt nanocrystal hybrids. (c) Size distributions of bare CG and CG−nanocrystal (NC) hybrids. (d) Measured size ranges of nanocrystals from SEM and TEM images.

process, polyvinylpyrrolidone (PVP) was used in the CG−Pt hybrid synthesis. The product Pt nanocrystals with PVP had a much smaller size as well as narrower size distribution when compared with Pt nanocrystals synthesized without the PVP surface surfactant (Supporting Information, Figure S2). On the basis of results of CG−Pt nanohybrids produced with and without PVP, it is concluded that surfactants can be used to control the size and morphology of nanocrystals in this aerosolization process, similar to its function for chemical reactions in an aqueous phase.

To investigate the crystalline structure of nanocrystals and also the interior structure of CG balls, TEM characterization (Figure 3) was performed on bare CG balls, CG−Mn_3O_4, and CG−SnO_2 hybrids. Figure 3a shows a typical CG ball structure, which is a three-dimensional structure with a folded graphene sheet. The formation of CG balls is driven by the capillary force associated with rapid solvent loss; the physical deformation naturally creates folds on the graphene surface. The TEM image clearly shows the folded structure, evidenced from the interlaced carbon lattices from the HRTEM image (Figure 3b). Figure 3c,d and Figure 3e,f show TEM and HRTEM images of CG−Mn_3O_4 and CG−SnO_2 hybrids, respectively. The images clearly show that both CG−Mn_3O_4 and CG−SnO_2 hybrids have a hollow structure with uniform nanocrystal decoration on both external and internal surfaces of the CG balls, which can be well understood since precursor ions initially adsorbed on both sides of the GO sheets before aerosolization. HRTEM images and SAED patterns confirm that the Mn_3O_4 and SnO_2 nanocrystals have a good crystalline structure. It was revealed that the lattice spacings of Mn_3O_4 nanocrystals are 0.49, 0.47, and 0.25 nm, which match well with the lattice spacings of tetragonal Mn_3O_4(111), (002), and (311), respectively.

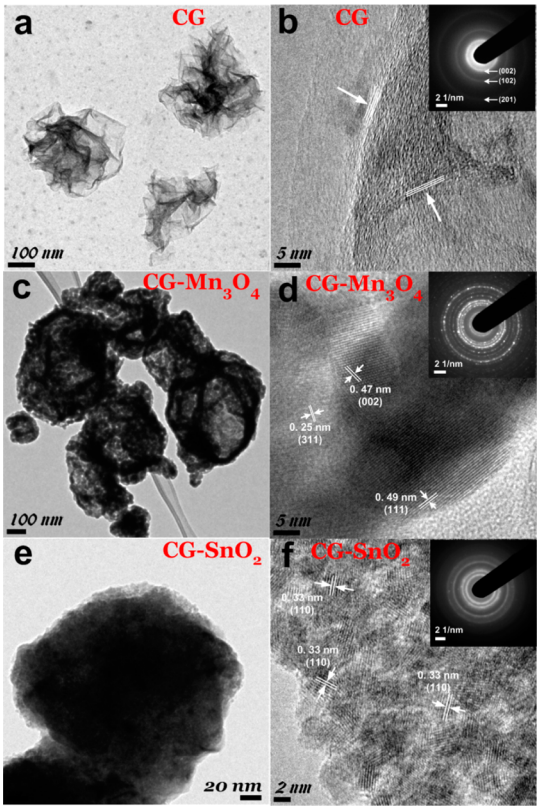

Figure 3. (a,b) TEM and HRTEM images of bare CG balls; (c,d) TEM and HRTEM images of CG−Mn_3O_4 nanocrystal hybrids; (e,f) TEM and HRTEM images of CG−SnO_2 nanocrystal hybrids.

The lattice spacings of SnO_2 nanocrystals are around 0.33 nm, which corresponds with the lattice spacing of rutile SnO_2(110). On the basis of HRTEM images, the size of the nanocrystals is determined as 20 ± 10 and 3 ± 1 nm for Mn_3O_4 and SnO_2, respectively. To further confirm the successful synthesis of CG−nanocrystal hybrids, element mapping and XRD measurements were carried out and the results are shown in Supporting Information, Figures S3 and S4.

According to the structure characterization of CG−nanocrystal hybrids, it is convincing that the aerosolization of GO suspension mixed with various precursors could serve as a general method to produce CG−nanocrystal hybrids. The present synthetic strategy shows great promise owing to the following advantages. First of all, the as-developed method can be carried out in one step and can be used for fabricating CG-based hybrids by loading various nanocrystals, including metals and metal oxides. Second, the size and morphology of the CG balls could be tuned by the size and thickness of initial GO sheets; and the size and the morphology of nanocrystals could be tuned by various parameters, such as the precursor concentration, aerosolization temperature, as well as the precursor source, which enables a deliberate synthetic design based on requirements of a specific application. Third, the CG balls are remarkably stable because such a crumpled ball is stabilized by locally folded, $\pi-\pi$ stacked ridges as a result of plastic deformation, which can withstand redispersion in an aqueous solvent without unfolding or collapsing the structure.[15] Fourth, because the crumpled structure of CG balls bears a higher specific surface area than commonly used flat GO/graphene papers, and a hollow/open structure facilitates the nanocrystal assembly on both external and internal surfaces of the CG balls, it is believed that this unique hybrid structure can be potentially useful for various applications. Last but not least, such nanohybrids can be directly deposited on the surface of a specified substrate without binder assistance and additional processing steps. For instance, in our preliminary experiments, ITO, copper foil, nickel foam, and carbon cloth were used as substrates to prepare nanohybrid electrodes for supercapacitors and lithium-ion batteries.

CG−Mn_3O_4 Hybrids for an Electrochemical Supercapacitor. As a proof of concept, we first investigated electrochemical properties of CG−Mn_3O_4 hybrids collected onto an ITO substrate and explored its potential application as the active electrode in electrochemical capacitors (ECs). Depending on the charge storage mechanism as well as the active materials used, ECs can be categorized into three types: electric double-layer capacitors (EDLCs), pseudocapacitors, and hybrid electrochemical capacitors.[20] On one hand, EDLCs store charges electrostatically *via* reversible ion adsorption at the electrode/electrolyte interface; the crumpled graphene is therefore expected to show attractive EDLC properties due to its high specific surface area. On the other hand, manganese oxides (MnO_x) is one of the transition metal oxides that is typically used as active pseudocapacitive materials because of its high theoretical specific capacitance (C_{sp} ~ 1370 $F \cdot g^{-1}$).[21] By combining these two types of materials, it is anticipated that a high-performance capacitor can be obtained as a result of both EDLC and pseudocapacitor mechanisms.

The electrochemical properties of the as-prepared CG−Mn_3O_4 hybrid were studied by performing cyclic voltammetry (CV) using a three-electrode cell system, as shown in the schematic of Figure 4a. The CG−Mn_3O_4 hybrid film on an ITO glass, which shows a brown color mainly resulting from the tetragonal Mn_3O_4 nanocrystals (Figure 4a), was used as the working electrode, and the Pt electrode and Ag/AgCl electrode were used as the counter electrode and the reference electrode, respectively. Figure 4b shows CVs for a CG−Mn_3O_4 electrode over a range of scan rates of 5−100 $mV \cdot s^{-1}$ with a potential window range of −0.6−1.2 V *versus* the Ag/AgCl reference electrode. The voltammetric curves show two pairs of peaks that correspond to the series of electrochemical redox reactions of Mn ions. The first pair of peaks in the range of −0.25−0.18 V could be attributed to the electrochemical conversion between the low valence state manganese ions (Mn^{2+} and Mn^{3+}), while

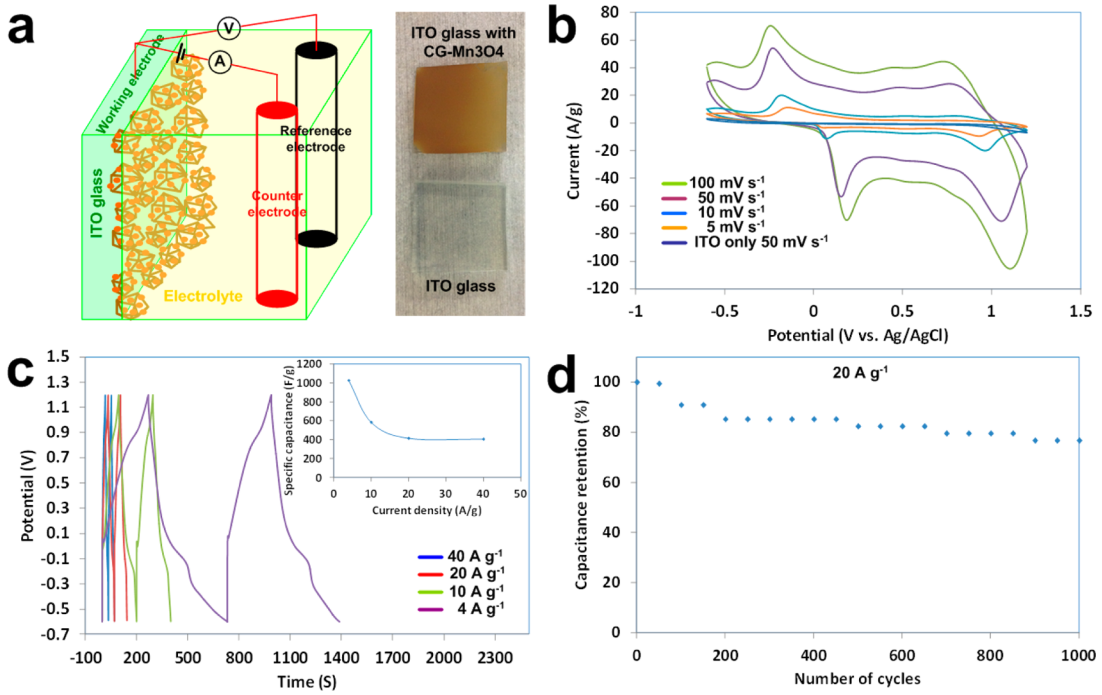

Figure 4. (a) Schematic of the capacitor test for CG−Mn_3O_4 nanocrystal hybrid electrode in a 1.0 M Na_2SO_4 aqueous electrolyte; digital pictures show the ITO glass before and after coating CG−Mn_3O_4 nanocrystal hybrids. (b) Cyclic voltammograms for CG−Mn_3O_4 at different scan rates (CV curve for ITO-only at a scan rate of 50 mV·s^{-1} is included for comparison). (c) Galvanostatic charging/discharging curves measured with different current densities for the assembled hybrid EC. The inset curve shows the calculated specific capacitance at different current densities. (d) Cycling performance of hybrid ECs at a current density of 20 A·g^{-1}.

the coupled peaks appearing at 0.75−1.10 V could be attributed to the redox reaction of high valence state manganese ions (Mn^{5+} and Mn^{7+}). On the basis of anodic and cathodic peaks, it is expected that the manganese ions undergo reversible oxidation and reduction reactions in the electrolyte during CV measurements, and detailed reactions may need further characterizations to indentify.[21−25] As the scan rate increases from 5 to 100 mV·s^{-1}, the peak current increases accordingly and the shape of the CV curves shows a little distortion accompanied by the shift of the anodic and cathodic peaks' position, which can be ascribed to the relatively slow kinetics of the reaction on the Mn-based oxides.[20] It should be noted that, at the same scan rate (50 mV·s^{-1}), the ITO-only electrode showed no peak in the scan windows and presented a much lower current density than that of the CG−Mn_3O_4, indicating that the modification of the high-surface-area CG balls with Mn_3O_4 did significantly enhance the specific capacity of EDLCs and pseudocapacitors.

Galvanostatic charge−discharge measurements were also carried out on the CG−Mn_3O_4 at different current densities, and the results are shown in Figure 4c. It can be seen that the charging curves are basically symmetrical with their corresponding discharge counterparts, and the results are in good agreement with that of the CV characterization. The specific capacitance is calculated from the discharge curves (see Supporting Information for more details). At a low current density of 5 A·g^{-1}, the specific capacitance can reach as high as 1027 F·g^{-1}, which is superior to or comparable with other high-performance GO/graphene/CNT-MnO_x hybrid nanostructure-based chemical capacitors (308−1250 F·g^{-1}).[20,21,26−29] The inset of Figure 4c shows the specific capacitance as a function of current density for the CG−Mn_3O_4 hybrids. The results indicate that CG−Mn_3O_4 hybrids not only deliver a high specific capacitance but also maintain a good rate capability at a high current density. Actually, a specific capacitance of 404 F·g^{-1} (40% retention) was retained at a current density as high as 40 A·g^{-1}. The electrochemical stability of the CG−Mn_3O_4 was also evaluated using the galvanostatic charge−discharge technique at a current density of 20 A g^{-1}. It was demonstrated that, based on the cycling test, the CG−Mn_3O_4 maintained ~78% capacitance retention over 1000 cycles at a current density of 20 A·g^{-1}, which is comparable with those reported in previous work (typically 69−79% retention over 1000 cycles).[30,31] The loss of the capacity mainly results from dissolution of Mn_3O_4 or mechanical stripping of CG−Mn_3O_4 during ion adsorption/desorption. It should be noted that the cyclability of the crumpled CG−Mn_3O_4 could be further improved through annealing treatment or adjusting the loading of Mn_3O_4 on CG.

CG−SnO_2 Hybrids for Lithium-Ion Battery. As mentioned above, the proposed route can be extended to directly fabricate various electrodes based on CG−nanocrystal hybrids for energy devices, such as lithium-ion batteries (LIBs). Sn-based materials show appealing

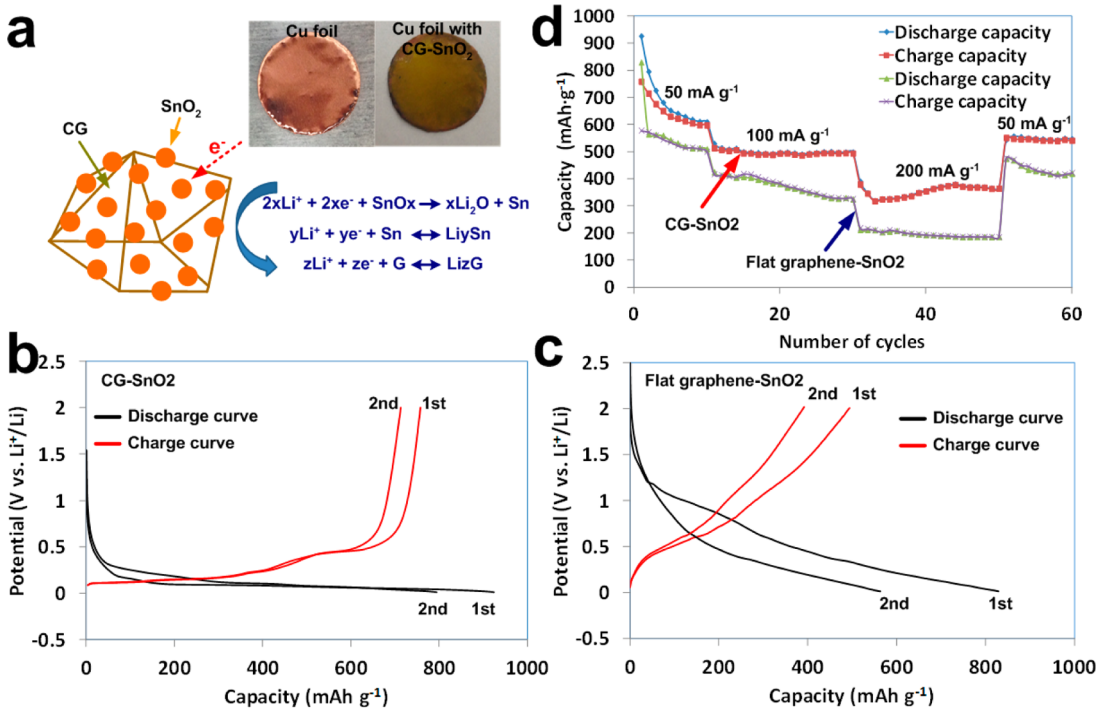

Figure 5. (a) Schematic of the LIB anode test for CG−SnO_2 nanocrystal hybrid on a copper foil. The initial two charge (red) and discharge (black) curves at a current density of 50 mA·g^{-1} for (b) CG−SnO_2 and (c) flat graphene−SnO_2. (d) Capacity retention of CG−SnO_2 and flat graphene−SnO_2 at various current densities.

properties of large capacity as anode materials in LIBs, and graphene-supporting Sn-based composites with various structures have been extensively investigated.[32,33] Here, CG−SnO_2 nanohybrids were directly deposited on a copper current collector (copper foil) without adding any binder and conductive carbon (Figure 5a). For comparison, the conventional flat graphene−SnO_2 nanohybrids were synthesized to fabricate LIB electrodes through minor modifications of a previous route.[34] A galvanostatic charge/discharge method was carried out to compare electrochemical properties of CG−SnO_2 nanohybrids and flat GO−SnO_2 as anodes in LIBs. Figure 5b,c displays the initial two charge−discharge curves for CG−SnO_2 and flat GO−SnO_2 nanohybrids, respectively. There are two observable plateaus ranging from 1.0 to 0 V in the first discharging process for both electrodes; these plateaus could be attributed to various reactions, including the transformation of SnO_2 and Li^+ to Sn and Li_2O, the formation of a series of Li−Sn alloys, and the Li insertion in graphene nanosheets (reactions (4)−(6)).

$$2xLi^+ + 2xe^- + SnO_x \rightarrow xLi_2O + Sn \quad (4)$$

$$yLi^+ + ye^- + Sn \leftrightarrow Li_ySn \quad (0 \le y \le 4.4) \quad (5)$$

$$zLi^+ + ze^- + G \leftrightarrow Li_zG \quad (6)$$

Obviously, there is a remarkable change between the first and the second discharge curve for the flat GO−SnO_2, indicating a large capacity loss in the initial two discharging processes. Such a result was somehow consistent with previous Sn-based anode materials ascribed to the irreversible reaction, volume expansion or pulverization, and the formation of a solid electrolyte interface (SEI) layer. Notably, the CG−SnO_2 nanohybrids display a much smaller change, signifying a much smaller capacity loss in the initial two cycles. Figure 5d compares the cycling performance and the rate capability of CG−SnO_2 nanohybrids and conventional flat graphene−SnO_2. Interestingly, the CG−SnO_2 nanohybrids exhibit a remarkable improvement in various performance parameters, including the specific capacity, rate capability, and stability. At first, the CG−SnO_2 nanohybrids display a capacity of 925.0 mAh·g^{-1} at a current density of 50 mA·g^{-1} in the first discharge process, which is much higher than that of flat graphene−SnO_2 (828.2 mAh·g^{-1}). Additionally, the initial capacity loss is about 15.2% in the CG−SnO_2 nanohybrids, while the flat graphene−SnO_2 exhibits a distinct fading of discharge capacity in the initial two cycles (around 33.5% loss). The reversible capacity decreased slowly with increasing current density. Even at a high rate of 200 mA·g^{-1}, CG−SnO_2 nanohybrids still delivered a specific capacity of about 380 mAh·g^{-1}, with a strong contrast to the flat graphene−SnO_2 that only has a corresponding capacity of 185 mAh·g^{-1}. Although the discharge capacity gradually decreased in the subsequent cycling, the CG−SnO_2 nanohybrids discharged a capacity of 545.96 mAh·g^{-1} and maintained this capacity in the following cycles when the current density was switched back to 50 mA·g^{-1}. However, it only delivered a capacity of 417.7 mAh·g^{-1} after 60 cycles for the flat graphene−SnO_2. Actually, the as-developed CG−SnO_2

nanohybrids also outperformed other graphene/CNT SnO_2-based LIB anodes.[35,36] The stable open structure in CG−SnO_2 nanohybrids could be a key factor responsible for the improved performance because such a unique nanostructure can greatly alleviate the volume change issue associated with SnO_2 anodes. Furthermore, several favorable properties of CG, such as good electrical conductivity and excellent mechanical properties, also can contribute to the enhanced performance.

There are several advantages arising from the GO aerosolization method to fabricate CG−nanocrystal electrodes for energy storage and conversion systems. At first, the electrode fabrication is completed in one single step, greatly decreasing the burden of electrode preparation. Second, the amount of active materials can be readily controlled through adjusting the concentration and aerosolization time of the suspension mixture, which provides a reliable strategy to optimize the corresponding performance for specific applications. Third, CG balls have an excellent stable structure in aqueous electrolyte and high accessible surface areas, which could be beneficial for rapid mass transfer of ions due to their open structure. Fourth, in this route, there are no binder and additional conductive agents needed to prepare the electrode. Moreover, because of the nature of the materials, the aerosolization method could be applied to assemble CG−nanocrystal hybrids onto various current colleting substrates, such as ITO glass, Cu foil, Ni foam, and carbon cloth (Figure S5, Supporting Information). As proved in our preliminary experiments, the CG−Mn_3O_4 and CG−SnO_2 hybrids showed excellent performance in applications of electrochemical supercapacitors and lithium-ion batteries. It is believed that the demonstrated devices with CG−nanocrystal hybrids can be further optimized by tuning the reduction level of GO, the size and distribution of the nanocrystals, and the loading of nanocrystals.

This novel aerosolization method is also promising for large-scale fabrication of electrodes using graphene−nanocrystal hybrids since it is a continuous manufacturing method and the material synthesis and assembly could be completed in one step. It should be noted that many types of inorganic nanomaterials could be prepared using this method and subsequently used for a broad range of applications including batteries, capacitors, catalytic systems, and sensors. For instance, CG−Pt hybrids could be used as a catalyst in fuel cell systems to catalyze methanol and formaldehyde oxidation reactions or oxygen reduction reactions, while CG−Ag hybrids are potentially useful in gas sensors. In addition, this method is expected to be extendable to GO/graphene−polymer hybrids with appropriate choice of precursor organics based on solubility and the drying temperature (organics can easily burn at high temperatures). A previous study showed that the CG structure could be achieved at low temperatures and even at room temperature.[19] Therefore, there is a huge potential in producing various crumpled graphene-based hybrids with different functionalities using this method, which offers another promising direction to develop graphene-based functional devices.

CONCLUSIONS

In summary, we have developed a general method to produce CG−nanocrystal hybrids through the aerosolization of GO suspension and precursor mixtures. Various nanocrystals including Mn_3O_4, SnO_2, Ag, and Pt were synthesized and decorated on the surface of CG balls during GO sheets evaporation and crumpling process. This method represents a general approach to one-pot fabrication of CG-based nanohybrid electrodes. As a demonstration, CG−Mn_3O_4 and CG−SnO_2 hybrid electrodes are fabricated and showed excellent performance in electrochemical supercapacitors and lithium-ion batteries. The method reported here offers huge opportunities in fabrication and applications of hybrid graphene−nanocrystal structures and opens up a new avenue for designing crumpled GO/graphene-based functional devices.

METHODS

Synthesis of CG−Nanocrystal Hybrids. Two types of GO were used in this study: monolayer GO ordered from Nanoinnova Technologies SL and multilayer GO produced from natural graphite powder using the modified Hummers method reported previously.[37] The monolayer GO sheet has a smaller lateral size ranging from tens of nanometers to two or three micrometers, and the multilayer GO has a larger lateral size in the range of tens of nanometers to more than ten micrometers. Monolayer GO was used in the hybrid nanostructure synthesis, and the multilayer GO was used as a comparison to investigate the difference in the resulting CG structure under the same experimental parameters. The GO suspension (0.2 mg GO/1 mL DI water) was prepared by dispersing the GO powder in DI water with the aid of ultrasonication. $Mn(NO_3)_2 \cdot 4H_2O$ (8.0 mM), $SnCl_4 \cdot 5H_2O$ (8.0 mM), $AgNO_3$ (8.0 mM), and H_2PtCl_6 (5.0 mM) were added into the GO suspension as precursors for the synthesis of CG−nanocrystal hybrids. To control the morphology and size of the Pt nanocrystal, polyvinylpyrrolidone (PVP) (2.0 $g \cdot L^{-1}$) was added and used as the surfactant. The mixed solutions were nebulized by an ultrasonic nebulizer (2.4 MHz, 241T, Sonaer) to form aerosol particles, which were carried by Ar/H_2 gas at a flow rate of 0.5 $L \cdot min^{-1}$ through a horizontal tube furnace preheated at a desired temperature (600−700 °C). An Ar and H_2 mixture (9:1) was used as the carrier gas for GO and $AgNO_3$; pure Ar gas was used for the other mixtures. The GO sheets were quickly dried and crumpled during flight in the tube furnace, and thermal decomposition or chemical reduction of precursors led to the formation of nanocrystals on the surface of GO sheets and resulted in a hybrid CG−nanocrystal structure. Si wafer, ITO glass (1 × 1 in.), Cu foil (0.25 in. diameter disk), Ni foam, and carbon cloth were used as substrates to collect the aerosol hybrid nanomaterials downstream of the tube. The typical collection time was 1−2 h. For CG−Mn_3O_4 and CG−SnO_2 hybrids, thermal annealing was carried out at 350 °C in Ar gas at a flow rate of 2 $L \cdot min^{-1}$ for 1 h to improve the crystallinity of nanocrystals.

CG−Nanocrystal Hybrid Characterization. The morphology of as-prepared samples, the selected area electron diffraction (SAED)

pattern, the energy-dispersive X-ray spectrum (EDS), and the elemental mapping were obtained using a Hitachi (H 9000 NAR) transmission electron microscope (TEM) and a Hitachi (S-4800) scanning electron microscope (SEM) equipped with an energy-dispersive spectroscopy analyzer. The size distributions of CG hybrids and nanocrystals were obtained by measuring and counting each hybrid structure in SEM and TEM images. Powder X-ray diffraction (XRD) was performed on a Scintag XDS 2000 X-ray powder diffractometer with monochromatized Cu Kα radiation (λ = 1.5418 Å); the data were collected between scattering angles (2θ) of 10 and 70°.

Electrochemical Supercapacitor and Lithium-Ion Battery Measurements. The electrochemical characterization was carried out using a CHI 600 electrochemical workstation (CHI Inc., USA). The three-electrode cell consisted of a Ag/AgCl electrode as the reference electrode, Pt as the counter-electrode, and the CG–Mn_3O_4 on ITO glass as the working electrode. A 1.0 M Na_2SO_4 solution served as the electrolyte in the three-electrode cell at room temperature. Cyclic voltammograms (CV) were carried out and recorded from −0.6 to 1.2 V at a scan rate of 5–100 $mV \cdot s^{-1}$. Galvanostatic charge–discharge measurements were performed with constant current densities from 5 to 50 $A \cdot g^{-1}$. Coin cells were assembled in an argon-filled glovebox for a lithium-ion battery. Lithium pellets were used for both the counter and the reference electrodes, and the CG–SnO_2 collected on a copper foil was directly used as a working electrode. The electrolyte solution was 1.0 M $LiPF_6$ dissolved in a mixture of ethylene carbonate (EC), dimethyl carbonate (DMC), and diethyl carbonate (DEC) with a volume ratio of EC/DMC/DEC = 1:1:1. Discharge–charge curves were recorded from 2.0 to 0.01 V at various current densities. Galvanostatic cycling experiments were conducted using a Land Battery Tester.

Conflict of Interest: The authors declare no competing financial interest.

Acknowledgment. Financial support for this work was provided by the U.S. National Science Foundation (CMMI-0900509) and the U.S. Department of Energy (DE-EE0003208). The authors thank Prof. M. Gajdardziska-Josifovska for TEM access at the HRTEM Laboratory of UWM, Dr. H. A. Owen for technical support with SEM analyses, and Dr. S. E. Hardcastle for technical support with XRD analyses. The SEM imaging was conducted at the Electron Microscope Laboratory of UWM. The XRD was conducted at the Advanced Analysis Facility of UWM.

Supporting Information Available: Characterization of CG produced from different GO sources, characterization of CG–Pt hybrids produced with and without PVP, element mapping data of CG–nanocrystal hybrids, XRD data of CG–Mn_3O_4 hybrids, and characterization of CG deposited on various substrates. This material is available free of charge *via* the Internet at http://pubs.acs.org.

REFERENCES AND NOTES

1. Dreyer, D. R.; Park, S.; Bielawski, C. W.; Ruoff, R. S. The Chemistry of Graphene Oxide. *Chem. Soc. Rev.* **2010**, *39*, 228–240.
2. Mao, S.; Pu, H.; Chen, J. Graphene Oxide and Its Reduction: Modeling and Experimental Progress. *RSC Adv.* **2012**, *2*, 2643–2662.
3. Park, S.; Ruoff, R. S. Chemical Methods for the Production of Graphenes. *Nat. Nanotechnol.* **2009**, *4*, 217–224.
4. Zhu, Y.; Murali, S.; Cai, W.; Li, X.; Suk, J. W.; Potts, J. R.; Ruoff, R. S. Graphene and Graphene Oxide: Synthesis, Properties, and Applications. *Adv. Mater.* **2010**, *22*, 3906–3924.
5. Kamat, P. V. Graphene-Based Nanoassemblies for Energy Conversion. *J. Phys. Chem. Lett.* **2011**, *2*, 242–251.
6. Pumera, M. Graphene-Based Nanomaterials for Energy Storage. *Energy Environ. Sci.* **2011**, *4*, 668–674.
7. Sun, Y.; Wu, Q.; Shi, G. Graphene Based New Energy Materials. *Energy Environ. Sci.* **2011**, *4*, 1113–1132.
8. Cote, L. J.; Kim, F.; Huang, J. Langmuir–Blodgett Assembly of Graphite Oxide Single Layers. *J. Am. Chem. Soc.* **2009**, *131*, 1043–1049.
9. Guo, F.; Kim, F.; Han, T. H.; Shenoy, V. B.; Huang, J.; Hurt, R. H. Hydration-Responsive Folding and Unfolding in Graphene Oxide Liquid Crystal Phases. *ACS Nano* **2011**, *5*, 8019–8025.
10. Guo, P.; Song, H.; Chen, X. Hollow Graphene Oxide Spheres Self-Assembled by W/O Emulsion. *J. Mater. Chem.* **2010**, *20*, 4867–4874.
11. Kim, K. S.; Zhao, Y.; Jang, H.; Lee, S. Y.; Kim, J. M.; Kim, K. S.; Ahn, J.-H.; Kim, P.; Choi, J.-Y.; Hong, B. H. Large-Scale Pattern Growth of Graphene Films for Stretchable Transparent Electrodes. *Nature* **2009**, *457*, 706–710.
12. Meyer, J. C.; Geim, A. K.; Katsnelson, M. I.; Novoselov, K. S.; Booth, T. J.; Roth, S. The Structure of Suspended Graphene Sheets. *Nature* **2007**, *446*, 60–63.
13. Patra, N.; Wang, B.; Kral, P. Nanodroplet Activated and Guided Folding of Graphene Nanostructures. *Nano Lett.* **2009**, *9*, 3766–3771.
14. Xu, Z.; Buehler, M. J. Geometry Controls Conformation of Graphene Sheets: Membranes, Ribbons, and Scrolls. *ACS Nano* **2010**, *4*, 3869–3876.
15. Luo, J.; Jang, H. D.; Sun, T.; Xiao, L.; He, Z.; Katsoulidis, A. P.; Kanatzidis, M. G.; Gibson, J. M.; Huang, J. Compression and Aggregation-Resistant Particles of Crumpled Soft Sheets. *ACS Nano* **2011**, *5*, 8943–8949.
16. Ma, X.; Zachariah, M. R.; Zangmeister, C. D. Crumpled Nanopaper from Graphene Oxide. *Nano Lett.* **2012**, *12*, 486–489.
17. Ruoff, R. A Means to an End. *Nature* **2012**, *483*, S42–S42.
18. Bai, S.; Shen, X. Graphene-Inorganic Nanocomposites. *RSC Adv.* **2012**, *2*, 64–98.
19. Chen, Y.; Guo, F.; Jachak, A.; Kim, S.-P.; Datta, D.; Liu, J.; Kulaots, I.; Vaslet, C.; Jang, H. D.; Huang, J.; *et al.* Aerosol Synthesis of Cargo-Filled Graphene Nanosacks. *Nano Lett.* **2012**, *12*, 1996–2002.
20. Yu, G.; Hu, L.; Vosgueritchian, M.; Wang, H.; Xie, X.; McDonough, J. R.; Cui, X.; Cui, Y.; Bao, Z. Solution-Processed Graphene/MnO_2 Nanostructured Textiles for High-Performance Electrochemical Capacitors. *Nano Lett.* **2011**, *11*, 2905–2911.
21. Kim, J.-H.; Lee, K. H.; Overzet, L. J.; Lee, G. S. Synthesis and Electrochemical Properties of Spin-Capable Carbon Nanotube Sheet/MnO_x Composites for High-Performance Energy Storage Devices. *Nano Lett.* **2011**, *11*, 2611–2617.
22. Fang, M.; Tan, X.; Liu, M.; Kang, S.; Hu, X.; Zhang, L. Low-Temperature Synthesis of Mn_3O_4 Hollow-Tetrakaidecahedrons and Their Application in Electrochemical Capacitors. *CrystEngComm* **2011**, *13*, 4915–4920.
23. Hu, C.-C.; Hung, C.-Y.; Chang, K.-H.; Yang, Y.-L. A Hierarchical Nanostructure Consisting of Amorphous MnO_2, Mn_3O_4 Nanocrystallites, and Single-Crystalline MnOOH Nanowires for Supercapacitors. *J. Power Sources* **2011**, *196*, 847–850.
24. Jeong, Y. U.; Manthiram, A. Nanocrystalline Manganese Oxides for Electrochemical Capacitors with Neutral Electrolytes. *J. Electrochem. Soc.* **2002**, *149*, A1419–A1422.
25. Zhao, G.; Li, J.; Jiang, L.; Dong, H.; Wang, X.; Hu, W. Synthesizing MnO_2 Nanosheets from Graphene Oxide Templates for High Performance Pseudosupercapacitors. *Chem. Sci.* **2012**, *3*, 433–437.
26. Chen, W.; Rakhi, R. B.; Hu, L.; Xie, X.; Cui, Y.; Alshareef, H. N. High-Performance Nanostructured Supercapacitors on a Sponge. *Nano Lett.* **2011**, *11*, 5165–5172.
27. Fan, Z.; Yan, J.; Wei, T.; Zhi, L.; Ning, G.; Li, T.; Wei, F. Asymmetric Supercapacitors Based on Graphene/MnO_2 and Activated Carbon Nanofiber Electrodes with High Power and Energy Density. *Adv. Funct. Mater.* **2011**, *21*, 2366–2375.
28. Huang, H.; Wang, X. Graphene Nanoplate-MnO_2 Composites for Supercapacitors: A Controllable Oxidation Approach. *Nanoscale* **2011**, *3*, 3185–3191.
29. Yu, G.; Hu, L.; Liu, N.; Wang, H.; Vosgueritchian, M.; Yang, Y.; Cui, Y.; Bao, Z. Enhancing the Supercapacitor Performance of Graphene/MnO_2 Nanostructured Electrodes by Conductive Wrapping. *Nano Lett.* **2011**, *11*, 4438–4442.
30. Chen, S.; Zhu, J.; Wu, X.; Han, Q.; Wang, X. Graphene Oxide-MnO_2 Nanocomposites for Supercapacitors. *ACS Nano* **2010**, *4*, 2822–2830.

31. Wu, Z.-S.; Ren, W.; Wang, D.-W.; Li, F.; Liu, B.; Cheng, H.-M. High-Energy MnO_2 Nanowire/Graphene and Graphene Asymmetric Electrochemical Capacitors. *ACS Nano* **2010**, *4*, 5835–5842.
32. Liang, S.; Zhu, X.; Lian, P.; Yang, W.; Wang, H. Superior Cycle Performance of Sn@C/Graphene Nanocomposite as an Anode Material for Lithium-Ion Batteries. *J. Solid State Chem.* **2011**, *184*, 1400–1404.
33. Wang, G.; Wang, B.; Wang, X.; Park, J.; Dou, S.; Ahn, H.; Kim, K. Sn/Graphene Nanocomposite with 3D Architecture for Enhanced Reversible Lithium Storage in Lithium Ion Batteries. *J. Mater. Chem.* **2009**, *19*, 8378–8384.
34. Wen, Z.; Cui, S.; Kim, H.; Mao, S.; Yu, K.; Lu, G.; Pu, H.; Mao, O.; Chen, J. Binding Sn-Based Nanoparticles on Graphene as the Anode of Rechargeable Lithium-Ion Batteries. *J. Mater. Chem.* **2012**, *22*, 3300–3306.
35. Wen, Z.; Wang, Q.; Zhang, Q.; Li, J. *In Situ* Growth of Mesoporous SnO_2 on Multiwalled Carbon Nanotubes: A Novel Composite with Porous-Tube Structure as Anode for Lithium Batteries. *Adv. Funct. Mater.* **2007**, *17*, 2772–2778.
36. Yao, J.; Shen, X.; Wang, B.; Liu, H.; Wang, G. *In Situ* Chemical Synthesis of SnO_2-Graphene Nanocomposite as Anode Materials for Lithium-Ion Batteries. *Electrochem. Commun.* **2009**, *11*, 1849–1852.
37. Mao, S.; Yu, K.; Cui, S.; Bo, Z.; Lu, G.; Chen, J. A New Reducing Agent To Prepare Single-Layer, High-Quality Reduced Graphene Oxide for Device Applications. *Nanoscale* **2011**, *3*, 2849–2853.